Experimental on physical properties of shale gas under low-velocity seepage and stress sensitivity environment

Yuliang Su[1,2], Chengwei Wang[1,2], Lei Li[1,2], Wendong Wang[1,2*], Yongmao Hao[1,2], S Rezaei-Gomari[3]

[1] Key Laboratory of Unconventional Oil & Gas Development (China University of Petroleum (East China)), Ministry of Education, Qingdao 266580, P. R. China

[2] School of Petroleum Engineering, China University of Petroleum (East China), Qingdao, 266580, P. R. China

[3] School of Science, Engineering and Design, Chmistry and Chemical Engineering Department, Teesside University-United Kingdom

*Corresponding authors: wwdong@upc.edu.cn

Abstract:

Shale gas reservoirs have complex pore structures, consisting not only of nanopores within and between organic grains but also of microcracks distributed randomly within the matrix. Although free gas and adsorption gas coexist, free gas is stored in pore spaces, and adsorption gas is stored in organic matter and clay minerals. Due to the presence of organic matter and heterogeneity in shale, the gas transfer mechanism is complicated involving multiple scales. Gas flow in shale does not conform to the characteristics of linear seepage at the low-velocity stage given the occurrence and flow state of different gases under different pressures. Meanwhile, very few studies have been performed on the low-velocity seepage characteristics of different gases in shale. Therefore, it is important to present experimental evidence for the low-velocity seepage law of different gases in shale. The present study uses experimental simulations of gas mass transfer at multi-scales to investigate the low-velocity gas flow and stress sensitivity of shale core samples. The results indicate that the shale matrix has a strong adsorption capacity, and that its helium flow capacity is 1.5~2.0 times greater than that of methane without backpressure. With increasing pore pressure, the combined action of gas adsorbed to the cavity and free gas leads to first an increase and then a decrease in the flow capacity of methane. With a low confining pressure, the permeability decreases exponentially. On the other hand, as the net confining pressure increases, the core fracture closes, causing the gas slip effect to increase permeability. The results of the study may provide valuable guidance in understanding gas flow in shale matrix and in the development of gas reservoirs.

Keywords: shale gas; slippage effect; low-velocity seepage; stress sensitivity

1 Introduction:

Analysis of world energy supply and demand in 2019 based on BP's Statistical Review of World Energy (2020)[1]. With the rapid development of the economy, human demand for energy is gradually increasing[2-3]. Based on BP's "world energy statistics yearbook", natural gas consumption has increased by 0.2% compared with 2018[4]. In the context of energy shortages and climate change, the development of shale gas has received considerable attention from the international community[5-6]. After the shale gas revolution occurred in the United States, countries around the globe have begun to develop shale gas resources on a large scale[7-10].

Shale gas reservoirs have strong anisotropy and heterogeneity[11-13]. A majority of pores in rocks are micropores with a diameter between 2 and 50 nanometers, mesopores with a diameter between 2 and 50 nanometers, and macropores with a diameter exceeding 50 nanometers[14-16]. Currently, there are three main methods for exploring the microscopic structure of shale gas pores, namely high-pressure mercury intrusion, nitrogen adsorption, and nuclear magnetic resonance[17-19]. Among them, the principal advantage of the high-pressure mercury intrusion technique is that it is a continuous test, the experimenter does not come in contact with mercury, and its safety is high[20-22]. During an experiment, the instrument automatically controls the entire experiment, while the experimenter can observe it at any time[23-25]. Nitrogen is adsorbed by capillary condensation in the pores of rock samples using the low-temperature nitrogen adsorption method[26-28]. During certain pressure conditions, the pores produce a single-layer adsorption phenomenon, and the specific surface area can be determined by calculating the adsorption data. Under conditions of constant temperature, the adsorption and desorption curves can be obtained by determining the relationship between changes in pressure and the amount of sample adsorbed. Following the calculation of the BJH equation, the adsorption-desorption curve of the sample is calculated, and the pore size distribution of the sample is determined[29-31]. Physically, nuclear magnetic resonance technology relies on the magnetic properties of hydrogen atoms and the interaction of external magnetic fields. To determine the rock pore structure and pore fluid, one reviews the relaxation rate and amplitude of the nuclear magnetic resonance relaxation signal of the hydrogen nuclear in the core pore fluid[32-34].

Researchers have so far used experimental methods to study the characteristics of shale gas seepage. The effect of shale bedding and rock relative permeability was studied by Ghanzaden et al, results indicate that, as shale matures, porosity and permeability parameters decrease first and then increase; at intermediate maturity, porosity and permeability reach their lowest value[35]. A study by Ghaohua Guo et al investigated nitrogen flow in nanofilms with pore throat sizes of 20 nm, 55 nm, and 100 nm[36]. According to the newly developed mathematical model, there is a significant difference between the apparent permeability and the inherent permeability in nanopores. As part of his research, Rasoul Nazari Moghaddm examined the permeability characteristics of shale gas under five different pore pressures and four net stresses[37]. The research results show that under any net stress, the matrix permeability

increases with the decrease of pressure due to the slip effect at the pore wall. Hui Han conducted CO_2 and N_2 adsorption experiments on the Longmaxi shale sample in the Sichuan Basin, and determined the pore volume and pore size distribution according to the gas adsorption[38]. Yufei Chen has studied the effects of isotropic stress and pore pressure on gas slip through experiments[39]. Yuling Tan used experimental methods to compare the permeability changes of shale gas cores under different saturation conditions and proposed a comprehensive permeability model considering the effects of water saturation, gas pressure and effective stress[40]. Using this model can more accurately describe the change law of wet core permeability under different gas pressures and in-situ stresses. Scholars such as Shaojie Zhang systematically measured the permeability, porosity, gas slip factor and gas diffusion coefficient of different shale samples under different confining pressures and pore pressures[41]. The research results show that as the confining pressure increases, the gas diffusion coefficient decreases exponentially, and the gas slippage factor increases exponentially. This research has improved the understanding of shale rock pressure sensitivity and gas slip and has important applications in the development of shale reservoirs. Due to the high content of clay minerals in shale gas reservoirs, natural fractures and complex pore structures are developed. As a result, a large amount of fracture fluid accumulates in the reservoir during the production process, forming a water phase trap, which in turn causes formation damage. Mingjun Chen and other scholars conducted formation water salinity analysis, stress sensitivity experiment, and velocity sensitivity analysis under different back pressure conditions. The perceptual experiment and the permeability experiment provide a basis for the determination of the aqueous phase trapping indoor experimental parameters. The research results show that the salinity of shale reservoir formation water is in the range of 2.258-8.46×10^4mg/L. The average value of formation water salinity is 5.5×10^4mg/L[42].

Through the velocity sensitivity experiment and stress sensitivity experiment, we understood that during the process, the control gradient is at 0.22MPa/cm, confining pressure control is at 10MPa, and the return pressure is at 10MPa. To accurately quantitatively characterize the pore structure and surface properties of shale gas reservoirs, Shangbin Chen selected Sichuan Longmaxi shale has been studied experimentally through TOC, XRD and LT-N_2GA[43]. A new shale porosity calculation method is proposed to calculate the contribution of different core components to shale porosity. The research results show that the average roughness of shale reservoirs with lower organic matter content is higher and the surface is rougher. At the same time, organic-rich shale has more pores and more complicated pore boundaries.According to the research on the contribution degree of shale porosity, the ranking of the contribution degree of shale reservoirs porosity is: organic matter, chlorite, potash feldspar and quartz[44].

According to numerous investigations results, the gas migration law under different seepage conditions in shale reservoirs is complicated. However, there are relatively few studies on the seepage characteristics of shale gas under various pore pressures and gas conditions. Therefore, in this paper, a

self-developed low-velocity shale gas seepage device is used to study the seepage characteristics of shale gas under low-velocity conditions and the stress-sensitive characteristics of matrix shale.

2 Experimental

2.1 Permeability measurements using pressure pulse decay method

Pressure pulse decay was used to measure all permeability measurements[45-46]. Helium was used as the test gas. The temperature of the permeability tests was kept constant at 25.5℃. A pump was used to apply confining pressure on the sample. the core holder was connected to an upstream gas chamber. The test procedure is as follows. Initially, the pressure exerted is the same everywhere in the system. A closed(main) value is less than the initial pressure that exists in the downstream chamber. The gas begins to flow under pressure and the pressure changes with time are recorded. The Δp versus time data series can then be analyzed to determine the sample permeability based on an analyzation to determine the sample permeability based on an analytical solution of the equations describing the pressure change during the experiment with known parameters of sample pore volume and gas properties. The experimental core is shown in Fig.1. The data on core pore permeability and gas properties are shown in Table 1and Table 2.

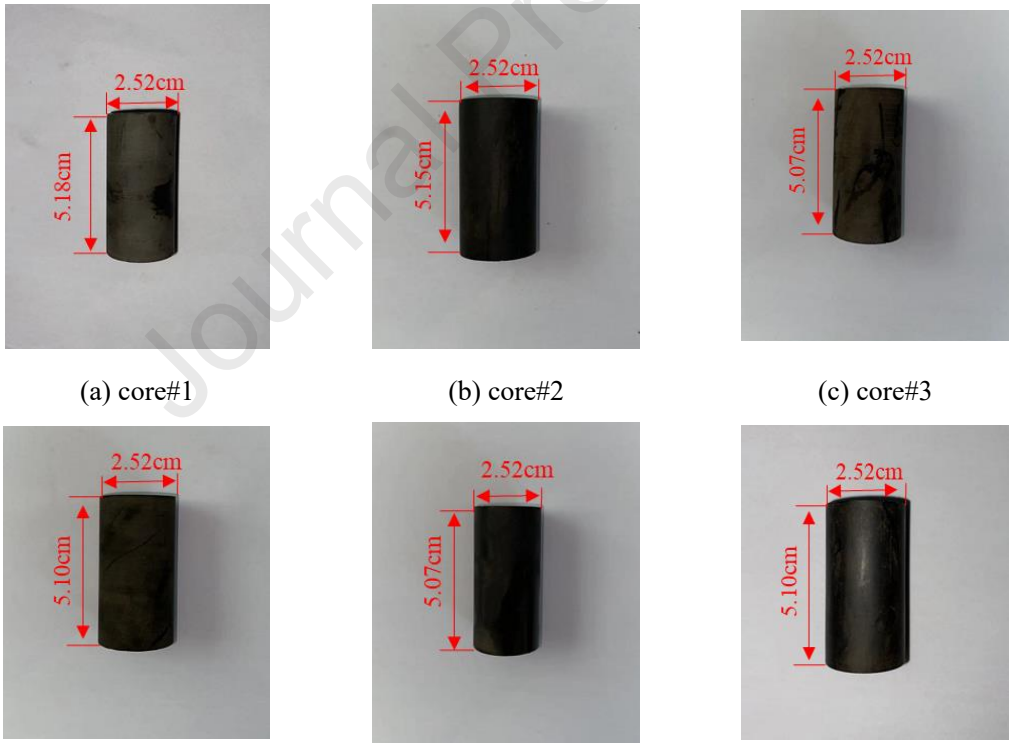

(a) core#1 (b) core#2 (c) core#3

(e) core#4 (f) core#5 (g) core#6

Fig.1 shale core sample used in this study

Table 1 porosity and permeability data of shale sample

Sample	Diameter,cm	Length,cm	Porosity, %	Permeability, md
Core#1	2.52	5.18	2.42	0.02298
Core#2	2.52	5.15	1.81	0.00164

Core#3	2.52	5.07	2.13	0.01409
Core#4	2.52	5.10	2.23	0.01862
Core#5	2.52	5.07	2.51	0.02364
Core#6	2.52	5.10	2.64	0.02371

Table 2 Gas properties

Gas	Molecular weight	Viscosity, Pa·s
Helium	4	1.89×10^{-5}
Methane	16	1.106×10^{-5}

2.2 Low-velocity seepage experiment for shale reservoir

To investigate low-velocity seepage of single-phase gas shale, methane, carbon and helium were used as gas media. Low-seepage law and characteristics of shale gas can be examined under a variety of conditions, including gas composition, pore pressure, and permeability. The schematic diagram of the experiment is shown in Fig.2. The experiment includes gas cylinder, pressure regulating system, self-made gas booster, self-made temperature-able core gripper, vacuum pump, backpressure valve, self-made six-way valve, self-made high-precision gas flow metering system and confining pressure pump. The experiment was carried out at reservoirs temperature (80℃), and the confining pressure was always higher than 5MPa at the inlet. Dry shale core was used as the experimental sample, and methane and helium were used as the experimental gas.

The detailed experimental steps are as follows.

(1) The core was placed in a core holder and the temperature was controlled at 80 ℃

(2) The core is vacuumed to saturate the gas.

(3) Adjust the gas pressure reducing valve to ensure that the pressure difference between the inlet end and the outlet end is 0.1-0.9MPa in turn, and the stabilization time of each pressure difference is at least 12h.

(4) The Darcy formula is used to calculate gas permeability, the formula is as follows:

$$K_{\mathrm{g}} = \frac{2Q_i p_0 \mu \mathrm{L}}{A(p_1^2 - p_2^2) \times 100}$$

K_g: Gas permeability,mD; Q_i: Gas flow, cm^3/s; p_0: atmospheric pressure, MPa; p_1: upstream pressure,MPa; p_2: downstream pressure, MPa. μ: viscosity, mPa·s; L: the length of the core, cm; A: Core cross-sectional area, cm^2.

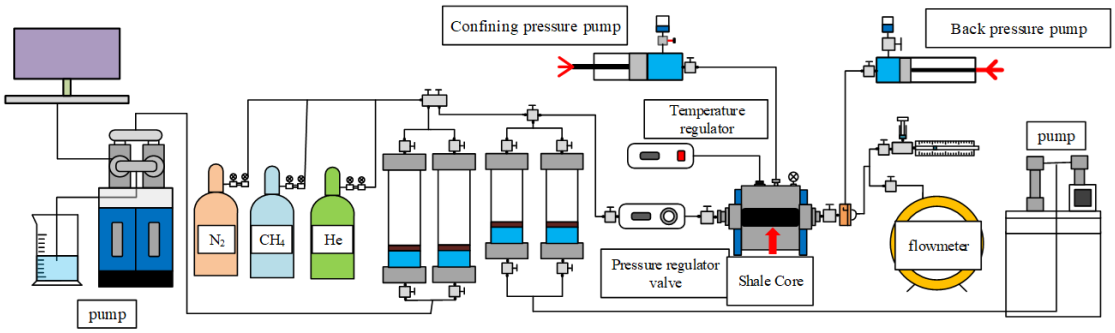

Fig.2 schematic diagram of low-velocity seepage experiment for shale reservoir

2.3 Experimental study on stress sensitivity of fracture shale reservoir

Since the physical characteristics of shale differ from those of sandstone, large-scale staged fracturing is necessary to increase the flow capacity of natural gas. This paper examines the stress sensitivity of shale samples under five different fracture morphologies. It was the same facility that was used for the low-velocity seepage experiment, the experiment was carried out under a temperature of 80°C. We chose Helium as the test gas, a high-precision plunger displacement pump was used to confine pressure equipment, and steady-state methods of gas seepage were utilized to conduct the test.

3 Result and discussion

3.1 Permeability test with methane and helium

As a result of the different gas properties, the characteristics of permeability variations caused by various gases in shale cores vary. The permeability of helium and methane at 80°C was studied. The experimental results are shown in Fig.3.

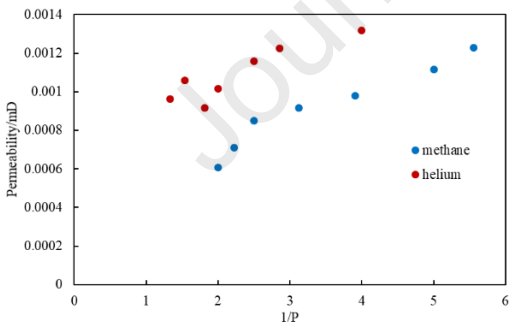

（a）permeability test with methane and helium(core#1)

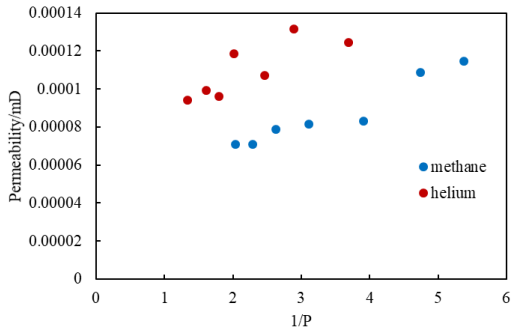

（b）permeability test with methane and helium(core#2)

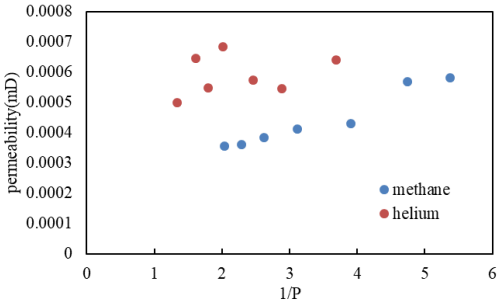

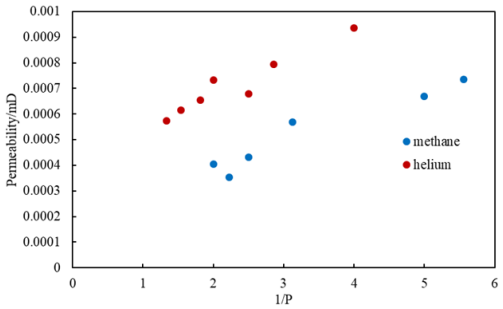

(c) permeability test with methane and helium(core#3)

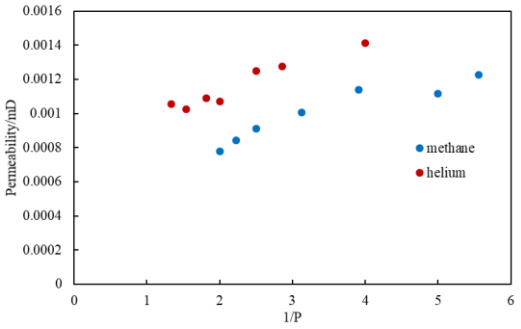

(d) permeability test with methane and helium(core#4)

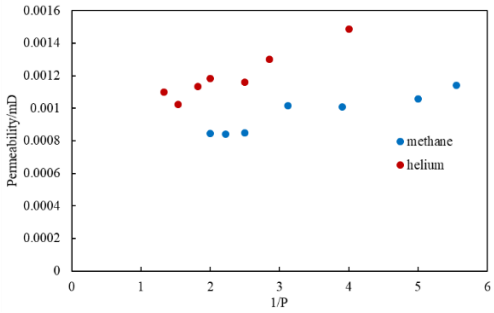

(e) permeability test with methane and helium(core#5)

(f) permeability test with methane and helium(core#*)

Fig.3 permeability test with methane and helium

The figure above illustrates that at the same pressure range, helium has a permeability that is 1.5~2 times greater than methane, which mainly caused by adsorption capacities of two kinds of gases. Considering the negligible capacity of helium to adsorb on shale reservoirs, the methane molecules are adsorbeed on the pore surface, forming a thick layer of adsorption. Adsorption layer thickness will reduce the gas flow channel, which will result in reduced pore permeability.

3.2 Permeability under different pressure

To avoid the effect of stress sensitivity on permeability change, a pressure difference of 5 MPa was maintained between the confining pressure and the inlet of the experiment. Once the gas flow at the outlet has stabilized, take a measurement of the gas flow, and then calculate the Darcy permeability using the Darcy formula.

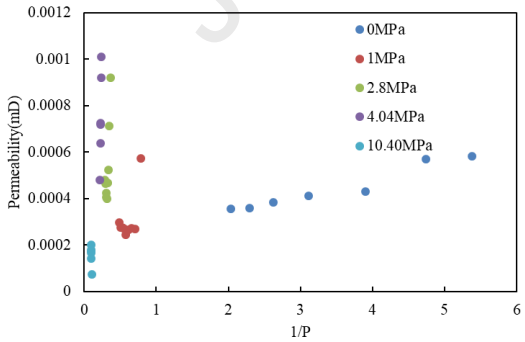

(a) Methane permeability in shale under different pore pressures(core#3)

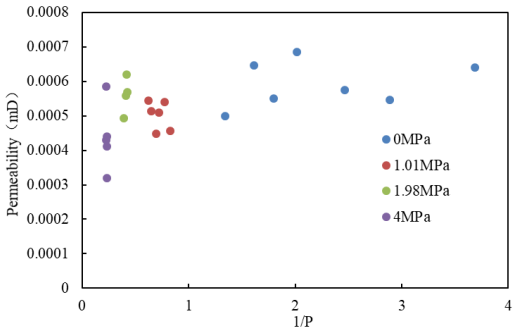

(b) Helium permeability in shale under different pore pressures(core#3)

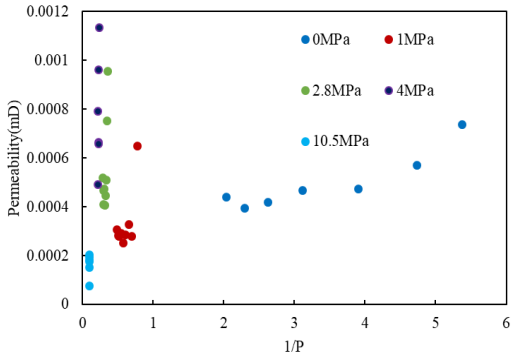

(c) Methane permeability in shale under different pore pressures(core#4)

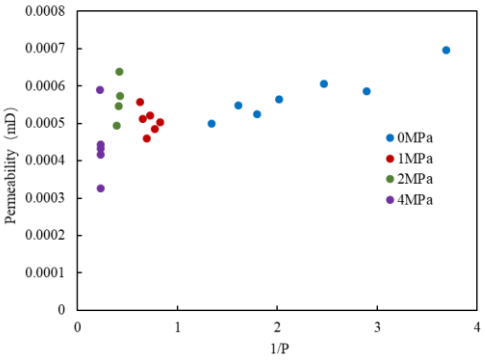

(d) Helium permeability in shale under different pore pressures(core#4)

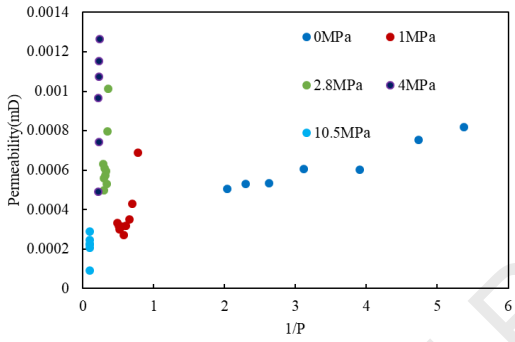

(d) Methane permeability in shale under different pore pressures(core#5)

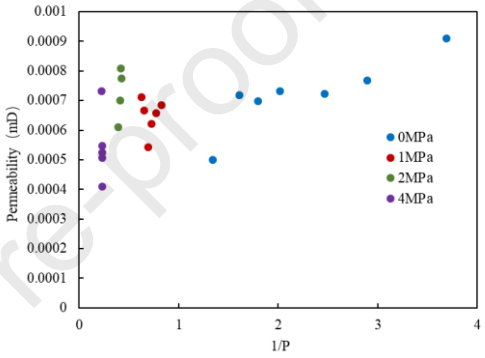

(e) Helium permeability in shale under different pore pressures(core#5)

Fig.4 Shale permeability under different pore pressure

During the experiment it was demonstrated that the seepage law of the matrix core varies under different backpressure conditions. According to the seepage law of the core, under conditions of zero and 10 MPa back pressure, the relationship is linear, while under conditions of 1 MPa and 2.8 MPa back pressure, the characteristic is clearly nonlinear. With increasing pore pressure, the methane permeability of the matrix core increased and then decreased, the permeability reaches its maximum value when the backpressure is about 5MPa. This phenomenon does not occur in helium gas permeability measurements under the same conditions. The permeability generally decreases with an increase in pore pressure, as shown in Figure 4.

By understanding the seepage law of gas in the core, we can know that the flow of gas in porous media is different from the flow of liquid. Generally speaking, gas in reservoirs exists in two states: free state and absorbed state, where the free state usually resides in fractures and pores, and the absorbed state usually adsorbs organic matter and its walls. In other words, the apparent permeability of organic porous media can be calculated as the sum of free gas permeability and adsorbed gas permeability. Matrix shale permeability is the result of two kinds of permeability. The apparent permeability of organic porous media can be expressed as[39].

$$K_{ad} = K_a + D\frac{\mu}{\rho}\cdot\frac{MC_{amax}p_L}{(p+p_L)^2(1-\Phi_{eff})}$$

K_{ad}: apparent permeability, mD; K_a: free gas permeability, mD; D: surface diffusion coefficient; M: molar mass of gas; C_{amax}: the density of the adsorbed phase at infinite pressure. μ: gas viscosity, mPa·s; P_L: Langmuir pressure, MPa; ρ: gas density, g/cm3; P: pore pressure, MPa; φ_{eff}: effective porosity

The change in permeability occurs primarily due to the adsorption of different gases in shale organic matter when the pore pressure remains unchanged. In comparison to the seepage characteristics of methane and helium, it can be observed that as pore pressure increases, the adsorption capacity of methane increases, resulting in the dominant permeability of the adsorbate layer. The permeability of the porous medium of organic matter has increased. As pore pressure increases, the adsorption capacity of organic matter to methane decreases. The adsorption layer thickness will not change with increased pore pressure when the saturation value is reached, and the apparent free gas permeability will prevail. With increasing pore pressure, the adsorption of shale organic matter to helium gas decreases. Meanwhile, the influence of free gas permeability increases, with the increase of pore pressure, the slippage effect is weakened and permeability gradually decreases.

3.3 The stress sensitivity of shale reservoirs

There are several types of fractured network, including fractures formed under natural conditions, artificial fractures without proppant filling, non-penetrating fractures, fractures perpendicular to the flow direction, and fractures filled with proppant. Fractures provide important conduits for the flow of oil and gas in shale reservoirs, and their conductivity impacts the production of oil and gas. This study was conducted by placing the plunger core into the fracturing apparatus, which was subsequently pressurized at a constant speed to create fractures of different shapes. A total of five kinds of fracture morphology are considered (nonpenetrating fractures, sanding fractures, longitudinal fractures, natural fractures, and artificial fractures). Figure 5 illustrates the fracture core diagram of two fracture types. As can be seen from the figure, the fracture occurs along one side of the core to produce artificial fractures and nonpenetrating fractures, respectively. The artificial fracture core is sanded with quartz particles to create sanding fractures, resulting in longitudinal fractures along the side of the core. The proppant is then slowly and uniformly injected into the spilt core to prepare the shale cores with various fracture shapes.

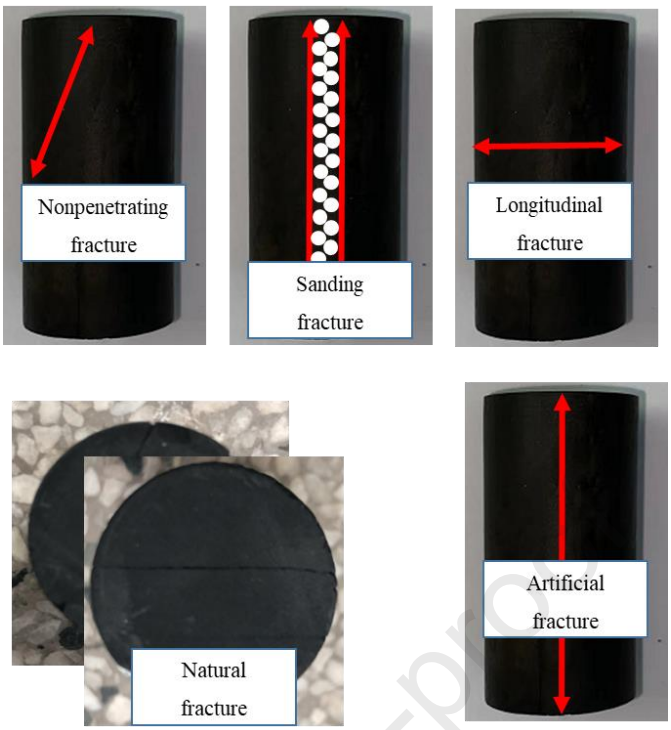

Fig. 5 Core diagram of different fractures

In addition, the shale gas stress sensitivity device was independently constructed to conduct an experiment on fracture cores of different types. The experimental results are shown in Fig.6、Fig.7、Fig.8、Fig.9 and Fig.10.

Table 3 Fracture core permeability data

Sample	Diameter, cm	Length, cm	fracture	Permeability, mD
Core#7	2.52	5.18	Nonpenetrating fracture	0.02298
Core#8	2.52	5.10	Sanding fracture	3.0153
Core#9	2.52	5.15	Longitudinal fracture	0.00164
Core#10	2.52	5.08	Natural fracture	1.0246
Core#11	2.52	5.12	Artificial fracture	2.4993

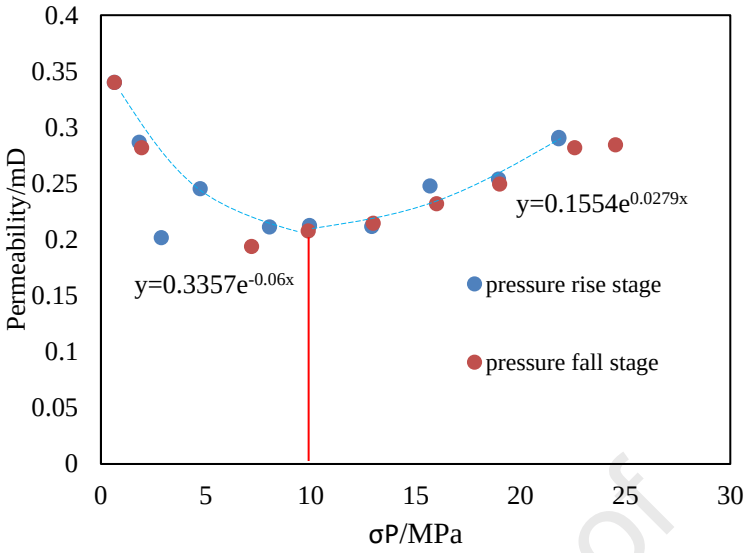

218

219 **Fig. 6 stress-sensitive curve of artificial fracture core**

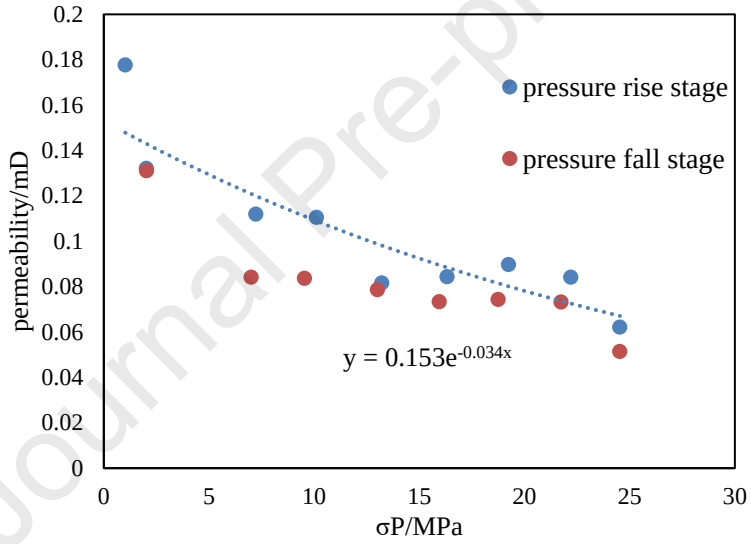

220

221 **Fig. 7 stress sensitivity curve of natural fracture core**

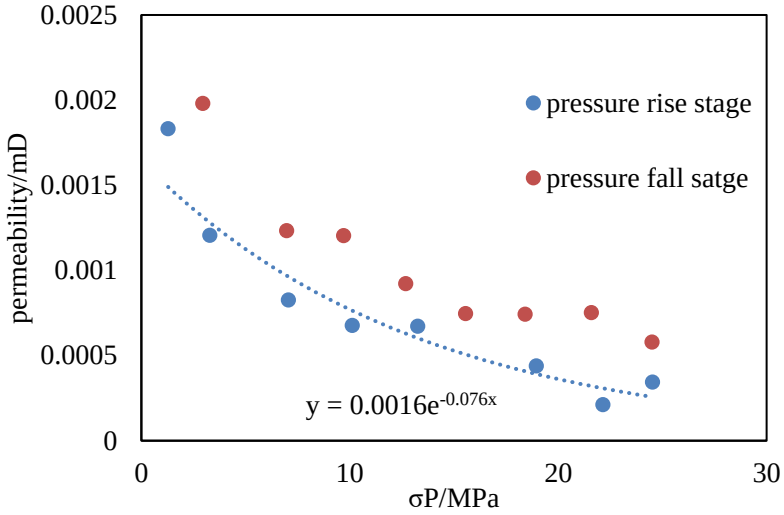

222

223 **Fig. 8 stress sensitivity curve of nonpenetrating fracture core**

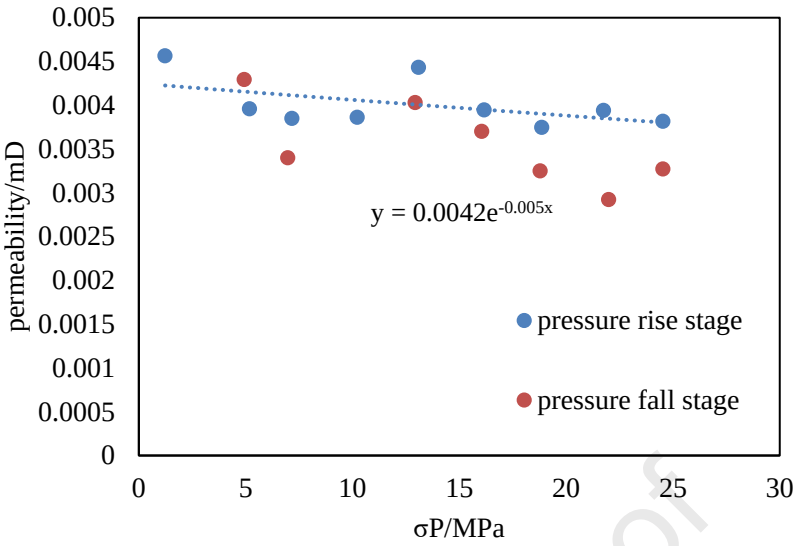

224

225 **Fig. 9 stress sensitivity curve of longitudinal fracture core**

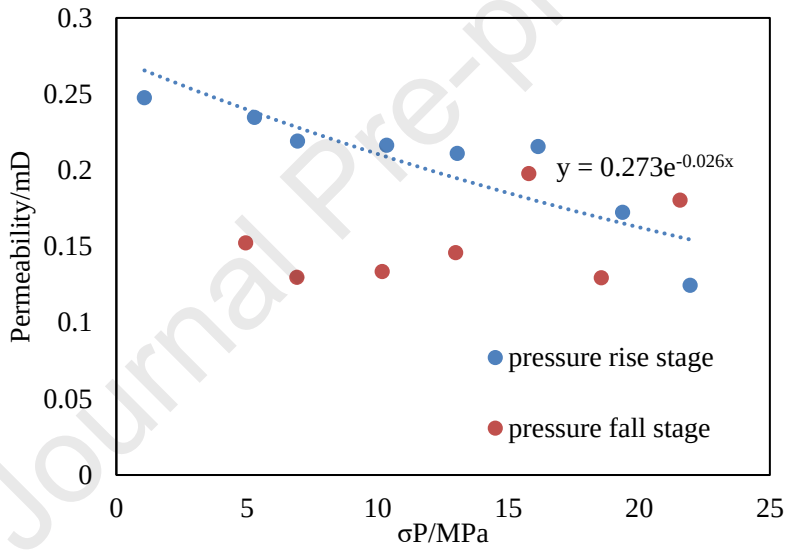

226

227 **Fig. 10 stress sensitivity curve of sanding fracture core**

228 Experimental results demonstrate that the stress sensitivity law varies with different fracture
229 morphologies of shale cores. According to the fitting of the stress sensitivity curve, the stress
230 sensitivity curve of the artificial crack shows a two-stage exponential distribution with a cut-off point
231 of 10 MPa, and the rest of the cores show an exponential distribution. The distribution function is
232 shown in Table 4.

233 **Table 4 Fracture core stress sensitivity function**

Sample	fracture	Distribution function
Core#1	Nonpenetrating fracture	$K=0.0016e^{-0.0766p}$
Core#2	Sanding fracture	$K=0.273e^{-0.0266p}$
Core#2	Longitudinal fracture	$K=0.0042e^{-0.0056p}$
Core#4	Natural fracture	$K=0.153e^{-0.0346p}$

Core#5	Artificial fracture	$K=0.3357e^{-0.066p}(\sigma p<10)$ $K=0.1554e^{0.02796p}(\sigma p<10)$

(a) Artificial fracture core (Fig. 6): The permeability of the fractured core decreases and then increases as core effective stress increases, because permeability is determined by both the degree of fracture closure, and by pore pressure. In the presence of high effective stress, the slip effect results in a decrease in permeability as the pore pressure increases. A low effective stress results in a decrease in fracture closeness, and permeability increases rapidly with a decrease in effective stress.

(b) Natural fracture core (Fig. 7): In the absence of a large core effective stress, the core fracture opens, and the permeability increases because the fracture has been opened. As the effective stress gradually closes. The permeability of a material changes slowly with stress when the effective stress reaches 15MPa because the crack is completely closed.

(c) Nonpenetrating fracture core (Fig. 8): The permeability of some non-penetrating joints increases when the effective stress is less than 10MPa.

(d) Longitudinal fracture core (Fig. 9): Upon finding longitudinal fractures in the core, gas is more difficult to pass through than the matrix and fracture core, resulting in a permeability that is not affected by changes in the effective stress.

(e) Sanding fracture core (Fig. 10): Permeability of paved sandstone core does not change significantly when effective stress changes.

4 Conclusion:

The low-velocity seepage law and stress sensitivity law of shale core are studied experimentally in this paper. Based on this study, the following conclusions can be drawn:

1. In shale, the seepage law varies depending on the microstructure of the shale and the state of the gas. Because the adsorption capacity of shale core to helium is weaker than that of methane, the permeability of helium is approximately 1.5 to 2 times greater than methane.
2. In accordance with the gas seepage law of shale cores, the permeability of shale consists of free gas permeability and adsorbed gas permeability. Under different pore pressures, two parts have different influence levels on permeability. When the pore pressure is 0~4MPa, with the increase of pore pressure, the permeability of adsorptive gas is enhanced, and the permeability of gas occupies a dominant position in the permeability of shale gas, eventually leading to the gradual increase of permeability. When the pore pressure is 4~10MPa, the adsorption gas content reaches the saturation value, and the free permeability dominates the shale gas permeability. Due to the slippage effect, the permeability decreases gradually as the pore pressure rises.
3. According to the stress-sensitivity experiments of different fracture cores, the stress-sensitivity characteristics of shale are different under different fracture morphology. Due to the high degree of artificial fracture fit, the fracture is completely closed when the net confining pressure of the core

is high. Due to the slippage effect, the shale permeability increases gradually with the increase of pore pressure. The stress-sensitive property of natural fracture and non-penetrating fracture core is similar to that of matrix shale and sandstone. With the increase of net confining pressure, permeability decreases gradually. The presence of longitudinal fractures in the core impedes gas flow to some extent, so that permeability does not fluctuate with the change of effective stress. The stress sensitivity of the sandstone core is relatively weak because the sand laying of the core can support the core.

Nomenclature

K_{ad} apparent permeability, mD

K_a free gas permeability, mD

D surface diffusion coefficient, dimensionless

m molar mass of gas, g/mol

C_{amax} the density of the adsorbed phase at infinite pressure, g/cm^3

μ gas viscosity, mPa·s

P_L Langmuir pressure, MPa

ρ gas density, g/cm^3

P pore pressure, MPa

$\varphi_{eff:}$ effective porosity, %

бp effective stress, MPa

Acknowledgments

The work is supported by the National Natural Science Foundation of China (51974348,51904324), and the National Science and Technology Major Project of China (ZD2019-183-007).

References

[1] Li H, Zhao S, Lin A, et al. Analysis on World Energy Supply & Demand in 2019-Based on BP Statistical Review of World Energy(2020)[J]. Natural Gas and Oil, 2020, 38(06): 122-130.

[2] YAO J, Sun H, Huang Z, et al. Key mechanical problems in the developmentof shale gas reservoirs[J]. Scientia Sinica Physica, Mechanica & Astronomica, 2013, 43(12): 1527-1547.

[3] Wei-yao Z H U, Zhen C, Zhi-yong S, et al. Research progress in theories and technologies of shale gas development in China[J]. Chinese Journal of Engineering, 2021, 43(10): 1397-1412.

[4] Taghavinejad A, Sharifi M, Heidaryan E, et al. Flow modeling in shale gas reservoirs: A comprehensive review[J]. Journal of Natural Gas Science and Engineering, 2020, 83: 103535.

[5] Wang Q, Chen X, Jha A N, et al. Natural gas from shale formation–the evolution, evidences and challenges of shale gas revolution in United States[J]. Renewable and Sustainable Energy Reviews, 2014, 30: 1-28.

[6] Zhao J, Ren L, Jiang T, et al. Ten years of gas shale fracturing in China: Review and prospect[J]. Natural Gas Industry B, 2022.

[7] Shangwen Zhou, Dazhong Dong, Jiehui Zhang, Chen Zou, Chong Tian, Yun Rui, Dexun Liu, Pengfei Jiao,Optimization of key parameters for porosity measurement of shale gas reservoirs,Natural Gas Industry B,Volume 8, Issue 5,2021,Pages 455-463, https://doi.org/10.1016/j.ngib.2021.08.004. (https://www.sciencedirect.com/science/article/pii/S2352854021000723)

[8] Wang Q, Li R. Research status of shale gas: A review[J]. Renewable and Sustainable Energy Reviews, 2017, 74: 715-720.

[9] Afagwu C, Mahmoud M A, Alafnan S, et al. Multiscale storage and transport modeling in unconventional shale gas: A review[J]. Journal of Petroleum Science and Engineering, 2022, 208: 109518.

[10] Hu Y, Liu G, Luo N, et al. Multi-field coupling deformation of rock and multi-scale flow of gas in shale gas extraction[J]. Energy, 2022, 238: 121666.

[11] Liu R, Jiang D, Zheng J, et al. Stress heterogeneity in the Changning shale-gas field, southern Sichuan Basin: Implications for a hydraulic fracturing strategy[J]. Marine and Petroleum Geology, 2021, 132: 105218.

[12] Liu Y, Liu S, Kang Y. Probing Nanomechanical Properties of a Shale with Nanoindentation: Heterogeneity and the Effect of Water–Shale Interactions[J]. Energy & Fuels, 2021, 35(15): 11930-11946.

[13] Xie J, Xiong W, Tan Y, et al. Effects of Anisotropic Permeability Evolution on Shale Gas Production: An Internal Swelling Factor Model[J]. Energy & Fuels, 2022, 36(2): 771-785.

[14] Ross D J K, Bustin R M. The importance of shale composition and pore structure upon gas storage potential of shale gas reservoirs[J]. Marine and petroleum Geology, 2009, 26(6): 916-927.

[15] Chen G, Lu S, Liu K, et al. Investigation of pore size effects on adsorption behavior of shale gas[J]. Marine and Petroleum Geology, 2019, 109: 1-8.

[16] Xu S, Gou Q, Hao F, et al. Shale pore structure characteristics of the high and low productivity wells, Jiaoshiba shale gas field, Sichuan Basin, China: Dominated by lithofacies or preservation condition?[J]. Marine and Petroleum Geology, 2020, 114: 104211.

[17] Talabi O, AlSayari S, Iglauer S, et al. Pore-scale simulation of NMR response[J]. Journal of Petroleum Science and Engineering, 2009, 67(3-4): 168-178.

[18] Kong X, Xiao D, Jiang S, et al. Application of the combination of high-pressure mercury injection and nuclear magnetic resonance to the classification and evaluation of tight sandstone reservoirs: A case study of the Linxing Block in the Ordos Basin[J]. Natural Gas Industry B, 2020, 7(5): 433-442.

[19] Li J, Du Y, et al. Classification Evaluation of Gas Shales Based on High-Pressure Mercury Injection: A Case Study on Wufeng and Longmaxi Formations in Southeast Sichuan, China[J]. Energy &

Fuels, 2021, 35(11): 9382-9395.

[20] Zhang J, Tang Y, He D, et al. Full-scale nanopore system and fractal characteristics of clay-rich lacustrine shale combining FE-SEM, nano-CT, gas adsorption and mercury intrusion porosimetry[J]. Applied Clay Science, 2020, 196: 105758.

[21] Gao H, Cao J, Wang C, et al. Comprehensive characterization of pore and throat system for tight sandstone reservoirs and associated permeability determination method using SEM, rate-controlled mercury and high pressure mercury[J]. Journal of Petroleum Science and Engineering, 2019, 174: 514-524.

[22] Labani M M, Rezaee R, Saeedi A, et al. Evaluation of pore size spectrum of gas shale reservoirs using low pressure nitrogen adsorption, gas expansion and mercury porosimetry: A case study from the Perth and Canning Basins, Western Australia[J]. Journal of Petroleum Science and Engineering, 2013, 112: 7-16.

[23] Wei Y, Li J, Du Y, et al. Classification Evaluation of Gas Shales Based on High-Pressure Mercury Injection: A Case Study on Wufeng and Longmaxi Formations in Southeast Sichuan, China[J]. Energy & Fuels, 2021, , 35(11): 9382-9395.

[24] Huang H, Chen L, Dang W, et al. Discussion on the rising segment of the mercury extrusion curve in the high pressure mercury intrusion experiment on shales[J]. Marine and Petroleum Geology, 2019, 102: 615-624.

[25] Omari A, Wang C, Li Y, et al. The progress of enhanced gas recovery (EGR) in shale gas reservoirs: A review of theory, experiments, and simulations[J]. Journal of Petroleum Science and Engineering, 2022: 110461.

[26] Han M, Wei X, Zhang J, et al. Influence of structural damage on evaluation of microscopic pore structure in marine continental transitional shale of the Southern North China Basin: A method based on the low-temperature N2 adsorption experiment[J]. Petroleum Science, 2021.

[27] Zhao P, Wang X, Cai J, et al. Multifractal analysis of pore structure of Middle Bakken formation using low temperature N2 adsorption and NMR measurements[J]. Journal of Petroleum Science and Engineering, 2019, 176: 312-320.

[28] Shi X, Wu W, Zhou S, et al. Adsorption characteristics and controlling factors of marine deep shale gas in southern Sichuan Basin, China[J]. Journal of Natural Gas Geoscience, 2022, 7(2): 61-72.

[29] Li J, Yin J, Zhang Y, et al. A comparison of experimental methods for describing shale pore features—A case study in the Bohai Bay Basin of eastern China[J]. International Journal of Coal Geology, 2015, 152: 39-49.

[30] Liu H, Farid I I, Sang S, et al. Synthetical study on the difference and reason for the pore structure of the No. 3 coal reservoir from the southern Qinshui Basin, China, using mercury intrusion porosimetry, low-temperature N2 adsorption, low field nuclear magnetic resonance, and nuclear

magnetic resonance cryoporometry[J]. Energy Reports, 2020, 6: 1876-1887.

[31] Yang X, Guo S. Comparative analysis of shale pore size characterization methods[J]. Petroleum Science and Technology, 2020, 38(14): 793-799.

[32] Wu Y, Liu C, Ouyang S, et al. Investigation of pore-throat structure and fractal characteristics of tight sandstones using HPMI, CRMI, and NMR methods: A case study of the lower Shihezi Formation in the Sulige area, Ordos Basin[J]. Journal of Petroleum Science and Engineering, 2022, 210: 110053.

[33] Sun W, Zuo Y, Wu Z, et al. Fractal analysis of pores and the pore structure of the Lower Cambrian Niutitang shale in northern Guizhou province: Investigations using NMR, SEM and image analyses[J]. Marine and Petroleum Geology, 2019, 99: 416-428.

[34] Fang T, Zhang L, Liu N, et al. Quantitative characterization of pore structure of the Carboniferous–Permian tight sandstone gas reservoirs in eastern Linqing depression by using NMR technique[J]. Petroleum Research, 2018, 3(2): 110-123.

[35] Ghanizadeh A, Gasparik M, Amann-Hildenbrand A, et al. Lithological controls on matrix permeability of organic-rich shales: an experimental study[J]. Energy procedia, 2013, 40: 127-136.

[36] Guo C, Xu J, Wu K, et al. Study on gas flow through nano pores of shale gas reservoirs[J]. Fuel, 2015, 143: 107-117.

[37] Moghaddam R N, Jamiolahmady M. Fluid transport in shale gas reservoirs: Simultaneous effects of stress and slippage on matrix permeability[J]. International Journal of Coal Geology, 2016, 163: 87-99.

[38] Han H, Cao Y, Chen S, et al. Influence of particle size on gas-adsorption experiments of shales: An example from a Longmaxi Shale sample from the Sichuan Basin, China[J]. Fuel, 2016, 186: 750-757.

[39] Chen Y, Jiang C, Leung J Y, et al. Gas slippage in anisotropically-stressed shale: An experimental study[J]. Journal of Petroleum Science and Engineering, 2020, 195: 107620.

[40] Tan Y, Zhang S, Tang S, et al. Impact of water saturation on gas permeability in shale: Experimental and modelling[J]. Journal of Natural Gas Science and Engineering, 2021: 104062.

[41] Zhang S, Sang Q, Dong M. Experimental study of pressure sensitivity in shale rocks: Effects of pore shape and gas slippage[J]. Journal of Natural Gas Science and Engineering, 2021, 89: 103885.

[42] Chen M, Lu Y, Kang Y, et al. Parameters selection for experiment on aqueous phase trapping damage in shale gas reservoirs[J]. Journal of Natural Gas Science and Engineering, 2020, 83: 103551.

[43] Chen S, Li X, Chen S, et al. A new application of atomic force microscopy in the characterization of pore structure and pore contribution in shale gas reservoirs[J]. Journal of Natural Gas Science and Engineering, 2021, 88: 103802.

[44] Li Z. Study on mechanism and model of shale gas flow in micro-nano pores[D]. China University of Petroleum, 2014.

[45] Sang. Experimental and Effective Production Conditions of Shale Oil and Gas[D]. China University of Petroleum(East China), 2017.

[46] Cui X, Bustin A M M, Bustin R M. Measurements of gas permeability and diffusivity of tight reservoir rocks: different approaches and their applications[J]. Geofluids, 2009, 9(3): 208-223.

Research highlights

- In this paper, low-velocity gas flow and stress sensitivity experiment of shale core samples were carried out based on the experimental simulation of gas multiscale mass transfer process.
- According to the experimental results, it can be seen that the shale matrix has a strong adsorption capacity, and the helium flow capacity is 1.5~2.0 times higher than that of methane with no backpressure.
- With the increase of pore pressure, the combined action of adsorbed gas and free gas leads to the methane flow capacity rise first and then decrease. When the confining pressure is small, the permeability decreases exponentially. However, as the net confining pressure increases, the core fracture is closed and the gas slip effect leads to the increase of permeability.